

Covalent Functionalization of Dipole-Modulating Molecules on Trilayer Graphene: An Avenue for Graphene-Interfaced Molecular Machines

Phong Nguyen, Junwen Li, T. S. Sreeprasad, Kabeer Jasuja, Nihar Mohanty, Myles Ikenberry, Keith Hohn, Vivek B. Shenoy,* and Vikas Berry*

The molecular dipole moment plays a significant role in governing important phenomena like molecular interactions, molecular configuration, and charge transfer, which are important in several electronic, electrochemical, and optoelectronic systems. Here, the effect of the change in the dipole moment of a tethered molecule on the carrier properties of (functionalized) trilayer graphene—a stack of three layers of sp^2 -hybridized carbon atoms—is demonstrated. It is shown that, due to the high carrier confinement and large quantum capacitance, the trans-to-cis isomerisation of ‘covalently attached’ azobenzene molecules, with a change in dipole moment of 3D, leads to the generation of a high effective gating voltage. Consequently, 6 units of holes are produced per azobenzene molecule (hole density increases by 440 000 holes μm^{-2}). Based on Raman and X-ray photoelectron spectroscopy data, a model is outlined for outer-layer, azobenzene-functionalized trilayer graphene with current modulation in the inner sp^2 matrix. Here, 0.097 V are applied by the isomerisation of the functionalized azobenzene. Further, the large measured quantum capacitance of 72.5 $\mu F cm^{-2}$ justifies the large Dirac point in the heavily doped system. The mechanism defining the effect of dipole modulation of covalently tethered molecules on graphene will enable future sensors and molecular-machine interfaces with graphene.

1. Introduction

Isomerizable molecules produce precise dipole modulation and nanoscale mechanics,^[1–7] which can be employed to build molecular valves,^[2,8] molecular hydroswitches,^[9] molecular cargo lifting,^[10] and molecular shuttles.^[11–13]

Similarly, several biosystems leverage molecular mechanics and dipolar behavior. For example, flagella strands (2–100 nm) on the outer cell wall of bacteria rotate to propel bacteria in solutions. Amongst mechanically actuating molecules, photoswitchable (photoisomerizable) molecules are interesting since these systems can be switched optically. The mechanics of these molecules are characterized by modulation of the dipole moment, response at high frequencies, and the absence of heat production. An extensively studied photoswitchable molecule is azobenzene, which photoisomerizes between *trans* and *cis* states, where the two configurations assume different dipole moments (*trans* = 0D; *cis* = 3D). There are several examples of electron-tunneling modulation through junctions with azobenzene;^[14–17] however, studies on its “covalent interfacing” to apply dipole-induced potential to change the carrier properties of the interfaced substrate are limited. In 2011, Kim et al.^[18] showed that azobenzene molecules attached vertically on graphene via π – π interfacing

P. Nguyen, Dr. T. S. Sreeprasad, K. Jasuja, N. Mohanty, M. Ikenberry, Prof. K. Hohn, Prof. V. Berry
 Department of Chemical Engineering
 Kansas State University, 66506, USA
 E-mail: vberry@k-state.edu

J. Li, Prof. V. B. Shenoy
 Department of Materials Science and Engineering
 University of Pennsylvania, 19104, USA
 E-mail: vshenoy@seas.upenn.edu



DOI: 10.1002/sml.201300857

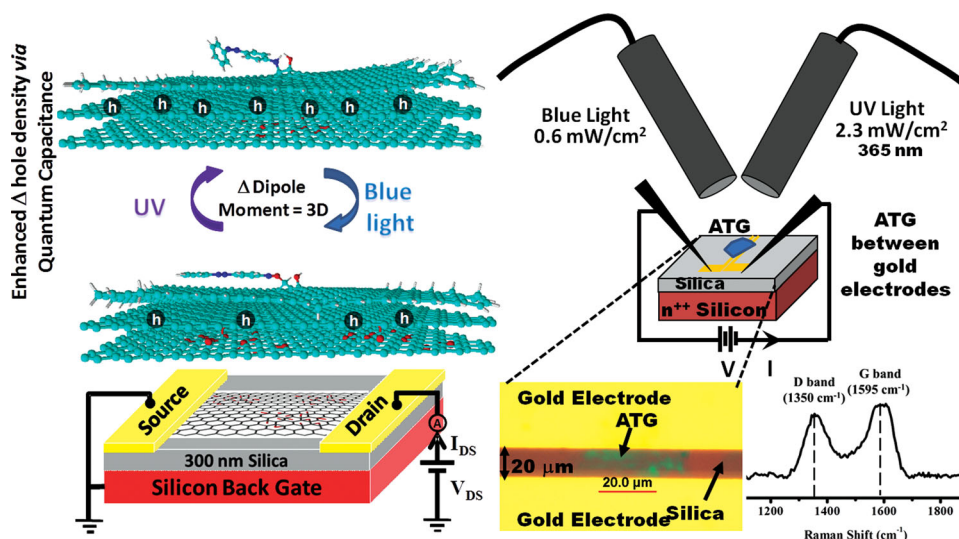


Figure 1. Representative model showing azobenzene molecules covalently bonded on the sp^3 regime of functionalized graphene. The azobenzene group changes its configuration on graphene (trilayer) when exposed to UV (cis) and blue light (trans). This mechanical motion of azobenzene modulates the density of holes in ATG. Bottom right: The optical image of ATG device between the gold electrodes $20\ \mu\text{m}$ apart. The Raman spectrum of the ATG sheet shows the D and G peak representing the graphenic backbone. Since graphene is functionalized, the Raman spectrum shows a D peak at $1350\ \text{cm}^{-1}$. No appreciable 2D peak was observed.

between pyrene and graphene can induce doping. However, noncovalent anchoring strategies (π – π interfacing, adsorption, etc.) are less robust under the conditions required for cleaning graphenic surfaces, such as annealing at high temperatures or joule heating under high vacuum.

In this contribution, we demonstrate that top and bottom layers of trilayer graphene (which are functionalized) can be leveraged as a platform to covalently bind azobenzene molecules at the top sp^3 regime with epoxy, $-\text{COOH}$, and $-\text{OH}$ groups. We discuss the functionalization process, structural/optoelectronic characterization, and conductivity-modulation model. In this stable, covalently functionalized azobenzene-trilayer-graphene (ATG) device, the electric field (and its polarity) from the molecular dipole moment of azobenzene, their configuration and orientation (normal component), as well as proximity with respect to graphene influences graphene's doping density (and/or carrier polarity). Hence, the devices exhibit robust and reversible carrier doping via a configurational change of azobenzene upon programmed UV/blue light exposure (**Figure 1**).

2. Device Fabrication

The device construct consists of a 300 nm silica dielectric layer on heavily doped n-type silicon back-gate with ATG deposited between two gold electrodes $20\ \mu\text{m}$ apart. Further, a monolayer (3-aminopropyl)triethoxysilane (APTES; Acros Organics) is used as a linker between silica (silane chemistry) and the bottom layer of ATG (via amide bond). Briefly, to fabricate the device, the silica substrate with gold electrodes is cleaned with water, acetone, ethanol, and isopropanol, dried, and exposed to oxygen plasma for 5 min (700 mTorr, 100 W). Subsequently, the substrate is submerged in 0.1% APTES in ethanol for 10 min to introduce positively

charged amine groups onto the silica surface. The chip is washed with 100% ethanol solution, dried, and baked in the oven at $120\ ^\circ\text{C}$ for 5 min to strengthen the bonds between silane and silica. To deposit the trilayer graphene (TLG) sheets across the gold electrodes, the chip is submerged in a GO solution for 15 min (see Supporting Information 1.a for GO preparation). This covalently binds GO to the substrate via amide bonds. Finally, the 4-aminoazobenzene molecule is tethered to the GO sheet via amide linkage by incubating the chip in 4-aminoazobenzene solution (1% aqueous) in the presence of 2-(1H-7-azabenzotriazol-1-yl)-1,1,3,3-tetramethyl uronium hexafluorophosphate Methanaminium (HATU) reagent^[19,20] for 12 h.

Here, the carboxylic and hydroxyl groups on the GO's exposed surface and the amine group on the 4-aminoazobenzene form amide bonds in the presence of the HATU catalyst (see Supporting Information 1.b for HATU procedure).^[19,21–22] Subsequently the unreacted oxy groups are reduced via hydrazine treatment (see Supporting Information 1.c) to produce ATG sheets spanning the electrodes. Finally the device is washed thoroughly with copious amount of water, acetone, and isopropanol to remove any residual hydrazine or adsorbed azobenzene. For subsequent calculation and analysis, the optimized orientation of the azobenzene molecule with respect to graphene was obtained from the ChemSketch program's molecular mechanics algorithm (**Figure 1**).

3. Results and Discussion

A typical device (**Figure 1**) consists of $\sim 35 \times 20\ \mu\text{m}^2$ ATG between gold electrodes. The Raman spectrum of a typical ATG sheet shows the D and the G peaks at 1350 and $1595\ \text{cm}^{-1}$, respectively. This indicates the presence of the

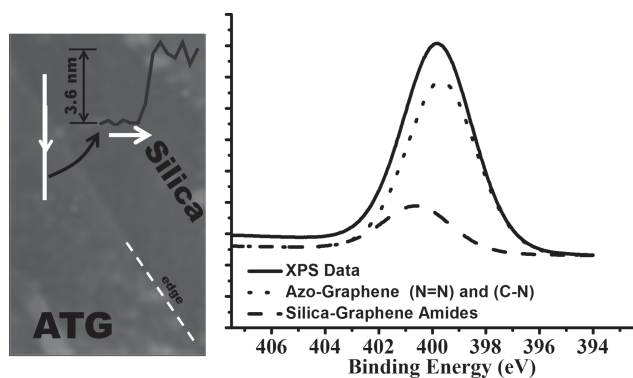


Figure 2. Left: AFM image ($1.7 \mu\text{m} \times 1 \mu\text{m}$) of a typical ATG sheet showing a height of 3.6 nm. Subtracting the height of the azobenzene and oxy groups, the underlying graphene is 3 sheets (including the two oxidized sheets). Right: The XPS spectrum of the ATG sheet shows the presence of the azo group. The peak at ~ 401.5 eV in ATG corresponds to the amide linkage ($\text{O}=\text{C}-\text{N}$) used to attach TLG to silica and 4-aminoazobenzene to GO. The peak at 400.5 eV corresponds $-(\text{C}-\text{N})-$ and $\text{N}=\text{N}$ in azobenzene.

graphenic backbone in ATG (Figure 1). No appreciable peak for 2D band was observed, as expected for functionalized graphene.^[23] Atomic force microscopy (AFM) analysis of the ATG devices gave a total thickness of 3.6 nm (left panel, **Figure 2**). Considering the height of the azobenzene group (0.31 nm), the remaining thickness corresponds to 3 graphene layers with two outer functionalized sheets and 1 inner graphene sheet.

X-ray photoelectron spectroscopy (XPS) data were recorded with a Perkin-Elmer PHI 5400 electron spectrometer using achromatic Al $K\alpha$ radiation (1486.6 eV). Analysis was carried out under a vacuum less than 5×10^{-9} Torr and heated to 120 °C to remove any adsorbed molecules on the surface. The XPS binding energies were measured with a precision of 0.025 eV. The analyzer pass energy was set to 17.9 eV, the contact time was 50 ms, and the area scanned was 4 mm². For the ATG, the peak for the amide bond ($\text{O}=\text{C}-\text{N}$) and the $\text{N}=\text{N}$ azo bond of azobenzene molecules appears around 401.5 eV and 400.5 eV respectively,^[24] while for the trilayer graphene (TLG, without azobenzene) the peak for the amide linkage with silica appears at around 401.5 eV^[25] (see Supporting Information Figure S2).

From XPS data analysis for the N and C peaks,

$$\frac{\#N}{\#C} = \frac{1}{16} = \frac{\frac{3a}{2} + c}{108 + 6a + 7b} \quad (1)$$

$$\frac{\#N_{\text{azobenzene}}}{\#N_{\text{silane}}} = \frac{4}{1} = \frac{\frac{3a}{2}}{c} \quad (2)$$

the azobenzene molecular density is 2.5 molecules nm⁻². Here: a is the number of N atoms in $\text{N}=\text{N}$ azobenzene molecules per nm², b is the number of N atoms in $\text{C}-\text{N}$ azobenzene molecules per nm² ($b = \frac{a}{2}$), and c is the number of N atoms in $\text{C}-\text{N}$ silane molecules per nm² (see Supporting Information Figure S3 and 4.c). The area of the azobenzene molecule is 0.27 nm² (or 3.7 per nm² of packed density), and

the total density of azobenzene molecule, $\rho_{\text{azo}} = 2.5$ per nm², calculated from XPS analysis (more details in the Supporting Information 4.c).

After confirming the anchoring of azobenzene on TLG, we studied the ATG device's optoelectronic behavior under UV/blue light exposure. As discussed earlier, graphene surface is ultrasensitive to the interfacial events and two primary explanations are discussed in the literature for this phenomenon:^[26] A) Graphene possesses a high quantum capacitance (for monolayer: $C_q = \frac{4e\pi^{\frac{1}{2}}}{h^2\pi^{\frac{1}{2}}(n_g + n_i)^{\frac{1}{2}}}$, where e is the electron charge, h is Planck's constant, φ_F is the Fermi velocity of the Dirac electron, and n_g and n_i are the carrier concentrations from the gate potential and the intrinsic carrier concentration of graphene, respectively);^[22] for a bilayer and trilayer:

$C_q = \frac{e^2 g_v g_s}{h^2 \pi \varphi_F^2}$, if Fermi energy (ϵ_F) is higher than the interlayer coupling (γ_l); for trilayer: $C_q = \frac{e^2 g_v g_s}{4h^2 \pi \varphi_F^2} (4\epsilon_F + \sqrt{2}\gamma_l)$, if $\epsilon_F < \gamma_l$. The quantum coupling of the interfacial molecules with graphene enhances the effective electric field due to the dipole moment of the molecules.^[27] The effective gating potential (ΔV_G), therefore, translates from a change in dipole voltage (ΔV_d) of the molecule to $\Delta V_G = f \left(\frac{C_q}{C_{\text{tot}}} \right) \Delta V_d$, where f is the fraction of sp^2 area which is gated by the azobenzene molecules. This was calculated using the equation $f = \left(\frac{2\pi r^2}{\sqrt{3}a^2} \right) = \rho_{\text{bulk}} A_{\text{azo}} = 2.5 \times 0.27 = 0.675$, where the bulk density of azobenzene $\rho_{\text{bulk}} = 2.5$ azo/nm² (calculated from XPS) and the area of one azobenzene molecule is $A_{\text{azo}} = 0.27$ nm². Also, $C_{\text{tot}} = (C_q^{-1} + C_g^{-1})^{-1}$ and C_g is the gate capacitance. B) Confined Doping: The change in the carrier concentration of graphene due to the change in the dipole moment of the molecule is amplified as a result of the confinement of the doped carriers within its ultrathin structure. The consortium of these properties makes graphene an ideal candidate for detecting interfacial molecular events.

Before the optoelectronic measurements, care was taken to remove adsorbed/nonbonded molecules (including any residual azobenzene, which can bind on graphene).^[28,29] All the ATG devices were electrically annealed (Joule heating = IVt ; 3 V for 5 min). Since high vacuum is not effective to avoid molecular desorption/adsorption,^[30] the device's optoelectronic response was characterized under a helium-pressure (19 psia) probe station with quartz optical windows; He adsorption on a graphene surface is negligible.^[31] The gold electrodes spanning ATG (source-drain) and silicon (back-gate) were connected to a dual-source meter (Keithley 2612). Each device was again electrically annealed (3 V for 30 min) under high He pressure to remove residual adsorbed impurities if any. The quartz optical ports were connected with UV (365 nm, power = 2.3 mW/cm²) and blue (420 nm, power = 0.6 mW/cm²) lamps to study the effect of UV and blue light exposures and dark (See **Figure 3**). The UV light isomerizes the azobenzene into its *cis* form (benzene rings closer to one another and a dipole moment of 3D), while blue light (or dark at room temperature) brings the azobenzene back to its *trans* form (benzene rings are opposite one another and have a dipole moment of 0D).

The optoelectrical measurements (Figure 3) show that the conductivity of the ATG device increases with exposure to UV, and reverts back to the original value with exposure to

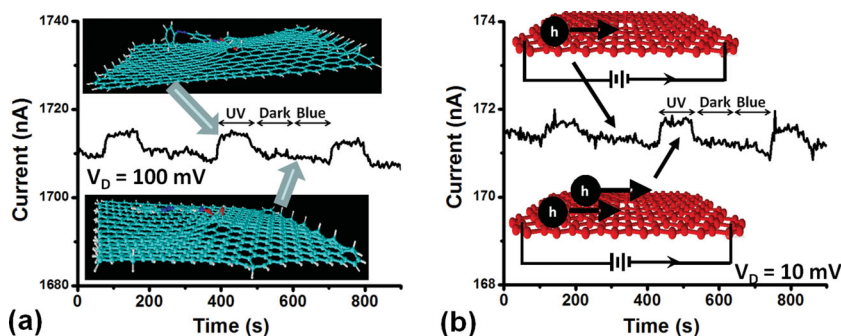


Figure 3. A) The figure shows the response of the ATG device (under 19 psia pure He environment at room temperature) exposed to UV, blue and dark for 90 s each at 100 mV source–drain voltage. (b) The same response (as (a)) is measured at 10 mV source–drain voltage. The current axis has been rescaled to better represent the change. Also, the azobenzene's *trans* configuration can be achieved via blue light exposure and temperature. Since, the rate of decrease of conductivity was not significantly more than that in dark environment; the room temperature is high enough to favor the *trans* state in the absence of UV. Further, it is known that the azobenzene could readily fluctuate between *cis* and *trans* configurations,^[32] leading to a fluctuation in current, as observed in electrical measurements.

blue light (420 nm) or in dark (UV/blue off), where the exposure time was 90 s each. The change in current for 100 mV and 10 mV source–drain voltage were 0.5 and 5 nA, which are directly scaled with the voltage (Figure 3a,b). This change in conductivity is attributed to doping of charge carriers in graphene due to a change in the dipole moment of the azobenzene. Here, the increase in dipole potential (due to 3D change in dipole moment) leads to hole doping in the *cis* configuration on the p-type (shown later) device. Further, the direct scaling of current modulation with voltage implies that the change in conductivity is not caused by desorption, the rate of which must increase with voltage due to Joule heating induced desorption. The measurements shown here are after several cycles of UV and blue exposures to equilibrate the response. Further, the *cis* to *trans* transition (under dark) is slower than *trans* to *cis* (UV on; see Supporting Information). A reduced graphene-oxide device (without azobenzene) did not show any discernible response to UV/blue exposure under similar conditions (see Supporting Information, Figure S4). The noise observed in the current measurements are expected to be a result of fluctuation in the configuration of the azobenzene, as has been discussed in several studies.^[32] To confirm the integrity of the sample after electrical measurements, XPS measurements were done, which gave similar scans to the ones before the optoelectronic measurements.

The carrier mobility and polarity in the ATG device were measured from back-gating studies using silicon as the back-gate and 300 nm silicon oxide as the gate oxide (Figure 4). The negative differential of the I_{DS} with V_G indicates that holes are the majority carriers (p-type device). The (average) slope of -2.22×10^{-2} nA/V implies a hole mobility of $0.195 \text{ cm}^2/\text{V/s}$ calculated via:

$$\mu = \frac{L \cdot d_{\text{SiO}_2}}{\bar{W} \cdot \epsilon \cdot \epsilon_0 \cdot V_D} \cdot \left(\frac{\Delta I_D}{\Delta V_G} \right)$$

Here, μ is the hole mobility, d_{SiO_2} is the thickness of silicon wafer, L is the channel length, \bar{W} is the average channel width, ϵ is the relative static permittivity of SiO_2 (~ 4), ϵ_0 is the permittivity of free space, V_D is the source–drain voltage, and $\left(\frac{\Delta I_D}{\Delta V_G} \right)$ is the absolute value of the linear slope of the back-gating curve.

Based on the carrier-mobility and hole dominant transport, we approximated the change in hole concentration due to the configuration change of the azobenzene-molecule. Here, the gating voltage ($|\Delta V_G|$) which induces the same change in current as the azobenzene mechanics (0.5 nA) is 34 V. This gating voltage provides the change in carrier density via the gate-capacitance equation: $\Delta q = C_{\text{SiO}_2} \cdot \left(\frac{|\Delta V_G|}{e} \right)$.

Here, Δq is the carrier surface density created due to azobenzene isomerization, and e is the elementary charge ($1.60 \times 10^{-19} \text{ C}$). This equation provides a value of $\sim 4.4 \times 10^5$ holes/ μm^2 generated due to the molecular-gating from UV-induced change of the azobenzene-molecule's configuration from *trans* to *cis*. With an azobenzene density of 2.5 nm^{-2} , this implies that mechanics of ~ 1 azobenzene molecule produces 6 holes. This corresponds to 15 quanta of hole generated per nm^2 of the base ATG. Also, the total carrier concentration at zero gate voltage is $3.3 \times 10^6 \mu\text{m}^2$ ($n_{\text{Total}} = \left(\frac{I_{DS}}{e \mu V_{DS}} \right)$).

To explain the mechanism of isomerization-induced doping in ATG, we use a simple model, which assumes that chemically exfoliated trilayer graphene comprises of two outer (top and bottom) functionalized (sp^3) and one middle graphene (sp^2) layer. In our system, the top layer is assumed to have a homogenous distribution of covalently bonded azobenzene and bottom is assumed to have oxy groups. Therefore, the electronic transport is dominant in the middle

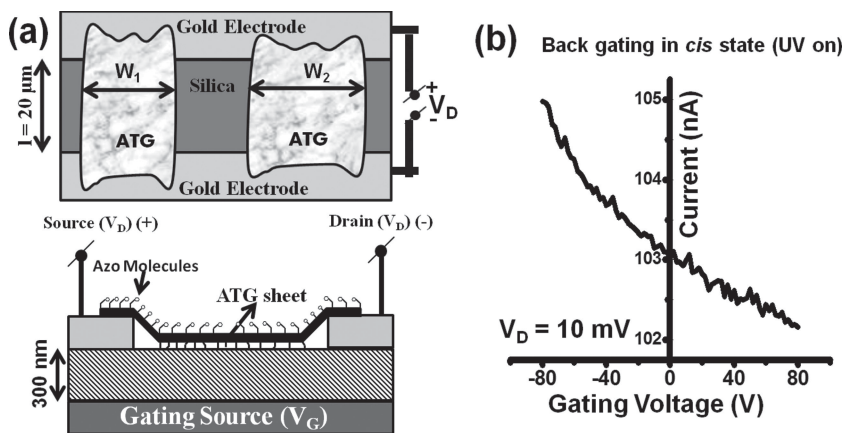


Figure 4. A) A schematic of the back gating measurement setup on device consisting of an ATG sheet spanning gold electrodes spaced $20 \mu\text{m}$ apart. The silica substrate, 300 nm , acted as a gate oxide, and heavily doped silicon acts as gate electrode. B) The gating study, conducted at 10 mV drain voltage, showed that the ATG device is p-type with a hole mobility of $0.195 \text{ cm}^2/\text{V/s}$. The measurement was made for the *cis* configuration of azobenzene in ATG.

graphene layer with azobenzenes on the top layer acting as molecular gates. Although, the charge mobility is high in sp^2 region, we observe a low value, which is attributed to the presence of a large density of charge traps from the functionalized groups in the top and bottom layers.

The dipole voltage induced on the middle graphene layer by azobenzene molecules via the change in dipole moment of the molecules (from *cis* to *trans* forms) is calculated by $\Delta V_d = [(\Delta\mu)\sin(\theta)/(4\pi\epsilon_0 r^2)][4\sum[i^2(\xi/r_{\text{Azo-Graphene}})^2 - 1]^{-3/2} + 3(i-1)\sum[3i^2/4(\xi/r_{\text{Azo-Graphene}})^2 - 1]^{-3/2}]$ where $\Delta\mu$ is the change in the dipole moment of azobenzene, i is the index (representing the distance of the dipole of the azobenzene and the point of interest), $r_{\text{Azo-Graphene}}$ is the distance between a dipole and middle-layer graphene, $\rho_{\text{packed-azo}}$ is the density of azobenzene molecules packed in top layer graphene oxide (3.7 azobenzene/nm²), and θ is the angle of inclination of the *cis*-azobenzene with respect of graphene ($\theta = 17.5^\circ$). The $\Delta\mu$ is calculated to be $3D$ ($3\sin(\theta) D = 0.92 D$), which yields an induced dipole voltage (ΔV_d) of 0.097 V.

The gating experiment shows that the change in conductivity via azobenzene's isomerization (0.5 nA at 10 mV V_{DS}) is also brought by 34 V of gating potential (see Supporting Information Figure S5). This implies that the change in the charge carriers for azobenzene isomerization through graphene's quantum capacitance is the same as that produced by gating: $\Delta V_G = f\left(\frac{C_q}{C_{\text{tot}}}\right)\Delta V_d$. This provides a quantum capacitance value of 72.5 $\mu\text{F}/\text{cm}^2$. Further, since the mobility of carriers in TLG is not expected to change with doping,^[31] our approximation of constant mobility with azobenzene-actuation is justified and consistent with earlier results on molecular-interfacing of few layer graphene with molecular moieties.^[19,31,33–35] The quantum capacitance of 72.5 $\mu\text{F}/\text{cm}^2$ provides a measure of the total carrier concentration ($fC_Q = \frac{4e\pi^2}{h\nu_F(n_{\text{Total}})^{1/2}}$), $n_{\text{Total}} = 3.19 \times 10^6 \mu\text{m}^{-2}$. This value is consistent with the total carrier concentration calculated from gating experiments ($3.3 \times 10^6 \mu\text{m}^{-2}$).

It was recently reported that the azobenzene's configuration change is faster, when it is incorporated into a thick GO composite where the tunneling distance between the sheets change.^[36] This although is a different mechanism, is consistent with the fast response of our ATG device. Further, our TLG devices without azobenzene does not show a discernible change in conductivity with UV or blue light exposure under the same conditions, confirming that the adsorption/desorption mechanism can be negated in the Helium environment. Our result, in combination with the case of vertically-oriented azobenzene on graphene^[18] showing reverse response, demonstrates that the polarity of doping is also dependent on the original orientation of azobenzene. We also show doping of graphene via π - π interfacing with perylene tetracarboxylic acid (see Supporting Information Figure S6).

4. Conclusion

In summary, we demonstrate that molecular mechanics (*trans* to *cis* configuration) of covalently anchored azobenzene (density = 2.5 nm⁻²) on trilayer graphene (37.5% sp^2 coverage) can sensitively and reversibly modulate its carrier

density (4.4×10^5 holes/ μm^2). Here, the change of $3D$ in the molecular dipole moment produces 0.097 V of dipole voltage, which leads to production of 6 quanta of hole per azobenzene molecule. The sensitivity evolves from the high quantum capacitance of 72.5 $\mu\text{F}/\text{cm}^2$. The total carrier density calculated from gating was consistent with that from quantum capacitance. We envision that this work will generate interest in applying graphene's sensitivity to molecular actuation and dependence on original orientation to develop rational interfaces with molecular machines (for example, rotaxane) and biomolecules for advanced applications in molecular switches, electromechanics, and protein folding. Futuristically, graphene nanoribbons devices interfaced with actuable molecules (proteins or molecular machines) could exhibit enhanced sensitivity.

Supporting Information

Supporting Information is available from the Wiley Online Library or from the author.

Acknowledgements

VB thanks the financial support from NSF (CMMI-1054877, CMMI-0939523 and CMMI-1030963), Office of Naval Research (grant-N000141110767), Terry C. Johnson Center for Basic Cancer Research, and KSU start-up.

- [1] N. Liu, Z. Chen, D. R. Dunphy, Y. B. Jiang, R. A. Assink, C. J. Brinker, *Angew. Chem. Int. Ed.* **2003**, *42*, 1731–1734.
- [2] S. Angelos, E. Choi, F. Vögtle, L. De Cola, J. I. Zink, *J. Phys. Chem. C* **2007**, *111*, 6589–6592.
- [3] T. Hugel, N. B. Holland, A. Cattani, L. Moroder, M. Seitz, H. E. Gaub, *Science* **2002**, *296*, 1103–1106.
- [4] P. L. Anelli, N. Spencer, J. F. Stoddart, *J. Am. Chem. Soc.* **1991**, *113*, 5131–5133.
- [5] J. D. Badjic, V. Balzani, A. Credi, S. Silvi, J. F. Stoddart, *Science* **2004**, *303*, 1845–1849.
- [6] M. Irie, *Chem. Rev.* **2000**, *100*, 1685–1716.
- [7] K. Jasuja, A. Thompson, V. Berry, *Small* **2008**, *4*, 2181–2186.
- [8] N. Liu, D. R. Dunphy, P. Atanassov, S. D. Bunge, Z. Chen, G. P. López, T. J. Boyle, C. J. Brinker, *Nano Lett.* **2004**, *4*, 551–554.
- [9] N. Delorme, J. F. Bardeau, A. Bulou, F. Poncin-Epaillard, *Langmuir* **2005**, *21*, 12278–12282.
- [10] V. Ferri, M. Elbing, G. Pace, M. Dickey, M. Zharnikov, P. Samorí, M. Mayor, M. Rampi, *Angew. Chem. Int. Ed.* **2008**, *47*, 3407–3409.
- [11] J. E. Green, J. W. Choi, A. Boukai, Y. Bunimovich, E. Johnston-Halperin, E. Delonno, Y. Luo, B. A. Sheriff, K. Xu, Y. S. Shin, H. R. Tseng, J. F. Stoddart, J. R. Heath, *Nature* **2007**, *445*, 414–417.
- [12] A. M. Brouwer, C. Frochet, F. G. Gatti, D. A. Leigh, L. Mottier, F. Paolucci, S. Roffia, G. W. Worpel, *Science* **2001**, *291*, 2124–2128.
- [13] N. Koumura, R. W. J. Zijlstra, R. A. van Delden, N. Harada, B. L. Feringa, *Nature* **1999**, *401*, 152–155.

- [14] B. Y. Choi, S. J. Kahng, S. Kim, H. Kim, H. W. Kim, Y. J. Song, J. Ihm, Y. Kuk, *Phys. Rev. Lett.* **2006**, *96*, 156106.
- [15] C. P. Collier, J. O. Jeppesen, Y. Luo, J. Perkins, E. W. Wong, J. R. Heath, J. F. Stoddart, *J. Am. Chem. Soc.* **2001**, *123*, 12632–12641.
- [16] M. J. Comstock, N. Levy, A. Kirakosian, J. W. Cho, F. Lauterwasser, J. H. Harvey, D. A. Strubbe, J. M. J. Frechet, D. Trauner, S. G. Louie, M. F. Crommie, *Phys. Rev. Lett.* **2007**, *99*, 038301.
- [17] Z. J. Donhauser, B. A. Mantooth, K. F. Kelly, L. A. Bumm, J. D. Monnell, J. J. Stapleton, D. W. Price, A. M. Rawlett, D. L. Allara, J. M. Tour, P. S. Weiss, *Science* **2001**, *292*, 2303–2307.
- [18] M. Kim, N. S. Safron, C. Huang, M. S. Arnold, P. Gopalan, *Nano Lett.* **2011**, *12*, 182–187.
- [19] N. Mohanty, V. Berry, *Nano Lett.* **2008**, *8*, 4469–4476.
- [20] N. Mohanty, M. Fahrenholtz, A. Nagaraja, D. Boyle, V. Berry, *Nano Lett.* **2011**, *11*, 1270–1275.
- [21] N. Mohanty, A. Nagaraja, J. Armesto, V. Berry, *Small* **2009**, *6*, 226–231.
- [22] P. Nguyen, V. Berry, *J. Phys. Chem. Lett.* **2012**, *3*, 1024–1029.
- [23] A. Kaniyoor, S. Ramaprabhu, *AIP Advances* **2012**, *2*, 032183.
- [24] L. Sharma, T. Matsuoka, T. Kimura, H. Matsuda, *Polym. Adv. Technol.* **2002**, *13*, 481–486.
- [25] E. Metwalli, D. Haines, O. Becker, S. Conzone, C. G. Pantano, *J. Colloid Interface Sci.* **2006**, *298*, 825–831.
- [26] T. S. Sreeprasad, V. Berry, *Small* **2012**, *9*, 341–350.
- [27] J. Xia, F. Chen, J. Li, N. Tao, *Nat. Nanotechnol.* **2009**, *4*, 505–509.
- [28] N. Peimyoo, J. Li, J. Shang, X. Shen, C. Qiu, L. Xie, W. Huang, T. Yu, *ACS Nano* **2012**, *6*, 8878–8886.
- [29] N. Peimyoo, T. Yu, J. Shang, C. Cong, H. Yang, *Carbon* **2012**, *50*, 201–208.
- [30] J. Lin, J. Zhong, J. R. Kyle, M. Penchev, M. Ozkan, C. S. Ozkan, *Nanotechnology* **2011**, *22*, 355701.
- [31] F. Schedin, A. K. Geim, S. V. Morozov, E. W. Hill, P. Blake, M. I. Katsnelson, K. S. Novoselov, *Nat. Mater.* **2007**, *6*, 652–655.
- [32] S. Yasuda, T. Nakamura, M. Matsumoto, H. Shigekawa, *J. Am. Chem. Soc.* **2003**, *125*, 16430–16433.
- [33] J. D. Fowler, M. J. Allen, V. C. Tung, Y. Yang, R. B. Kaner, B. H. Weiller, *ACS Nano* **2009**, *3*, 301–306.
- [34] I. Jung, D. Dikin, S. Park, W. Cai, S. L. Mielke, R. S. Ruoff, *J. Phys. Chem. C* **2008**, *112*, 20264–20268.
- [35] G. H. Lu, L. E. Ocola, J. H. Chen, *Appl. Phys. Lett.* **2009**, *94*, 083111.
- [36] X. Zhang, Y. Feng, P. Lv, Y. Shen, W. Feng, *Langmuir* **2010**, *26*, 18508–18511.

Received: March 18, 2013
Published online: